15-band spectral envelope function formalism applied to broken gap tunnel field-effect transistors

15-band spectral envelope function formalism applied to broken gap tunnel field-effect transistors

D. Verreck*, M. L. Van de Put†, A.S. Verhulst, B. Sorée †*, W. Magnus†,
A. Dabral*, A. Thean and G. Groeseneken*
imec, Kapeldreef 75, 3001 Leuven, Belgium
* Department of Electrical Engineering, KU Leuven, Belgium
† Department of Physics, Universiteit Antwerpen, Belgium
e-mail: devin.verreck@imec.be

***Abstract*— A carefully chosen heterostructure can significantly boost the performance of tunnel field-effect transistors (TFET). Modelling of these hetero-TFETs requires a quantum mechanical (QM) approach with an accurate band structure to allow for a correct description of band-to-band-tunneling. We have therefore developed a fully QM 2D solver, combining for the first time a full zone 15-band envelope function formalism with a spectral approach, including a heterostructure basis set transformation. Simulations of GaSb/InAs broken gap TFETs illustrate the wide body capabilities and transparant transmission analysis of the formalism.**

I. Introduction

The tunnel field-effect transistor (TFET) is often cited as a promising low-power alternative to the conventional metal-oxide-semiconductor field-effect transistor (MOSFET) [1], [2]. This is because the TFET subthreshold swing (SS) can go below 60 mV/dec at room temperature thanks to its operating principle based on band-to-band tunneling (BTBT). However, Si TFET on-currents (I_{on}) are typically too low, hindering actual circuit implementation. Therefore, heterostructures of III-V materials are under active investigation to improve the TFET I_{on} [3]–[9]. The band alignment of the heterostructure provides an additional degree of freedom to minimize the effective bandgap at the tunnel junction, thereby increasing tunneling probability. This is particularly true for the broken gap alignment, in which the effective bandgap is zero, which should allow for high I_{on}. However, preliminary quantum mechanical (QM) simulations have shown important reflections at the heterojunction [10]. Along with other quantum effects like field-induced and size-induced confinement, these reflections can heavily influence TFET performance. We have therefore developed a fully QM 2D ballistic formalism to investigate transport in heterostructure TFETs. The formalism combines a full-zone 15-band envelope function (EF) formalism, including a heterostructure basis set transformation, with a spectral approach. The spectral scheme keeps the computational burden bearable and prevents spurious solutions from polluting the zone-center. Additionally, we have developed an algorithm to obtain 15-band material parameters while retaining commutativity of the momentum matrices.

II. Formalism

Our formalism is based on the EF formalism with quantum transmitting boundary conditions [11]. In going to a 15-band description, we replace the finite difference (FD) scheme in the confined direction with a spectral approach, in which we expand the odd (F_n) and even (F_m) EFs, and the external potential V_e as follows:

$$F_n(x,z) = \sum_{\mu=-\infty}^{+\infty} \tilde{F}_n(x,k_{z\mu}) \sin(k_{z\mu} z) \tag{1}$$

$$F_m(x,z) = \sum_{\mu=-\infty}^{+\infty} \tilde{F}_m(x,k_{z\mu}) \cos(k_{z\mu} z) \tag{2}$$

$$V_e(x,z) = \sum_{\mu=-\infty}^{+\infty} \tilde{V}_e(x,k_{z\mu}) \cos(k_{z\mu} z) \tag{3}$$

$$
\begin{aligned}
\frac{-\hbar^2}{2m_e}\frac{\partial^2 \tilde{F}_n(x,k_{z\mu})}{\partial x^2} &+ k_y^2\frac{\hbar^2}{2m_e}\tilde{F}_n(x,k_{z\mu}) + k_{z\mu}^2\frac{\hbar^2}{2m_e}\tilde{F}_n(x,k_{z\mu}) \\
&- \frac{i\hbar}{m_e}\sum_{m''}\{\mathbf{p}_{nm''}(x)\}_x\frac{\partial \tilde{F}_{m''}(x,k_{z\mu})}{\partial x} \\
&+ k_y\frac{\hbar}{m_e}\sum_{m'}\{\mathbf{p}_{nm'}(x)\}_y\tilde{F}_{m'}(x,k_{z\mu}) \\
&\pm k_{z\mu}\frac{i\hbar}{m_e}\sum_{m}\{\mathbf{p}_{nm}(x)\}_z\tilde{F}_{m}(x,k_{z\mu}) \\
&+ \sum_{m'''}H_{nm'''}(x)\tilde{F}_{m'''}(x,k_{z\mu}) \\
+ \sum_{\mu'=0}^{+\infty}&\left[\tilde{V}_e(x,k_{z\mu'}-k_{z\mu}) \mp \tilde{V}_e(x,k_{z\mu'}+k_{z\mu})\right]\tilde{F}_n(x,k_{z\mu}) \\
&= E\tilde{F}_n(x,k_{z\mu}),
\end{aligned}
$$

Fig. 1. System of EF equations after the spectral transform. The plus(minus)-sign in the potential term corresponds to an even(odd) EF. m_e is the free electron mass. $\mathbf{p}_{nm}$ and H_{nm} represent the $\mathbf{k}\cdot\mathbf{p}$ interband momentum and Hamiltonian matrix elements respectively, which couple band n to band m. Note that the potential term becomes the sum of a convolution and an autocorrelation of the spectral components of the potential.

with x (z) the transport (confinement) direction, and translational invariance in y. The parity of the EFs is determined by the band coupling, with coupled EFs having opposite parity. Inserting Eqs. (1)-(3) in the EF system finally results in the following system of Fig 1.

If N_x x-grid points, N bands and N_{k_z} spectral components are considered, the system has dimensions $N_x \times N_{k_z} \times N$ after discretization, instead of $N_x \times N_z \times N$ in a FD approach. Since spectral methods provide exponential accuracy, compared to only polynomial accuracy for FD, N_{k_z} can be much lower than N_z, especially when the EFs vary slowly in the confined z-direction. Additionally, the cut-off in the spectral expansion prevents highly oscillating out-of-zone spurious solutions from polluting the first Brillouin zone (see Fig. 2). Fig. 3 shows the full simulation procedure.

III. 15-BAND PARAMETERS

In order to use the same EF basis set throughout the heterostructure, the matrix elements $\mathbf{p}_{nm}$ and H_{nm} (see Fig. 1) are transformed [11], [12]. This transformation requires a common eigenvalue decomposition, and therefore commutativity, of the momentum matrices. For the exact case of infinite bands, this is satisfied. Momentum matrix elements

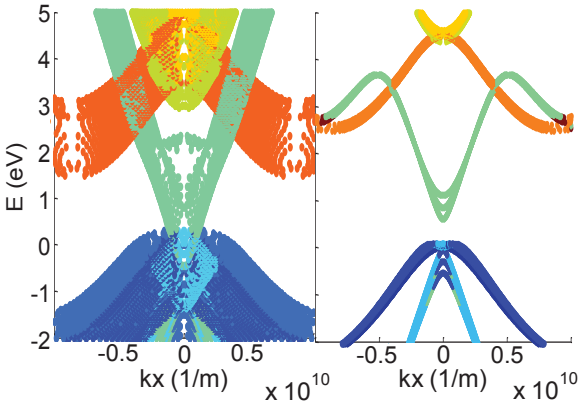

Fig. 2. 15-band confined band structure calculation for a 10 nm InAs slab using a finite difference scheme (left) and a spectral approach with 3 spectral components (right) in the confined z-direction. The spectral approach prevents spurious solutions from folding back onto the zone center and hence results in a correct confined band structure description. Colors indicate the dominant band contribution to each state.

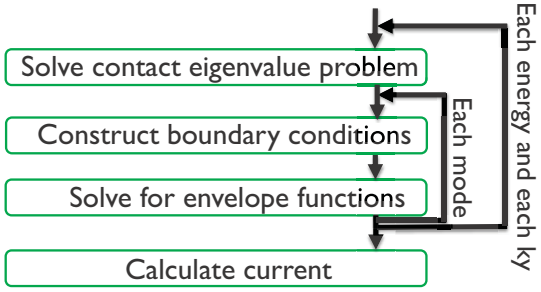

Fig. 3. Flowchart of the developed formalism.

in literature for finite band models, however, have lost this feature in the fitting process. We have therefore developed a constrained optimization algorithm, to search for $\mathbf{k}\cdot\mathbf{p}$-parameters that reproduce energy gaps and effective masses at the Γ-point and the energy gaps of the X-and L-valleys [13], while retaining commutativity of the momentum matrices (see Fig. 4). This enables the common eigenvalue decomposition and hence the basis set transform. The parameters that were obtained for GaSb and InAs are collected in Tables I and II.

IV. SIMULATION RESULTS

Figs. 5 and 6 show simulation results for a broken gap diode and p-n-i-n TFET. The computational efficiency of the spectral method permits the simulation of wide structures: one 30 nm body TFET

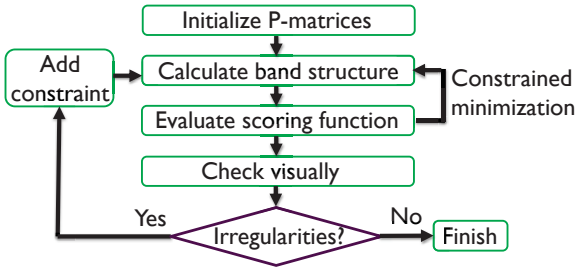

Fig. 4. Parameter search algorithm. The scoring function is a weighted sum of differences of calculated and experimental values from literature of effective masses and bandgaps at the Γ, X-and L-valleys. The constraints ensure commutativity of the momentum matrices P_x, P_y and P_z.

TABLE I

15-BAND **K·P** BASIS FUNCTIONS WITH CORRESPONDING ENERGY LEVELS, USING THE NOTATION OF *Radhia et al.* [14].

Basis function	GaSb [eV]	InAs [eV]
$\|S_V\rangle$	-12.13	-12.69
$\|X\rangle, \|Y\rangle, \|Z\rangle$	0	0
$\|S\rangle$	0.73	0.37
$\|X_c\rangle, \|Y_c\rangle, \|Z_c\rangle$	3.82	4.39
$\|S_u\rangle$	8.56	8.55
$\|D_x\rangle$	9.53	9.88
$\|D_z\rangle$	10.17	9.88
$\|X_d\rangle, \|Y_d\rangle, \|Z_d\rangle$	10.89	11.89
$\|S_q\rangle$	13.14	12.64

TABLE II

15-BAND **K·P** MOMENTUM MATRIX ELEMENTS IN UNITS OF ENERGY, USING THE NOTATION OF RADHIA *et al.* [14].

Matrix element	GaSb [eV]	InAs [eV]
E_P	19.89	20.75
E_{PX}	13.38	14.52
E_{P3}	3.26	3.11
E_{P2}	1.42e-09	1e-08
E_{PS}	6.52e-04	0.07
E_{Pd}	0.93	0.14
E_{PXd}	4.12	5.22
E_{P3d}	10.57	8.66
E_{P2d}	24.34	22.41
E_{PU}	17.50	19.67
$E_{P'}$	0	0

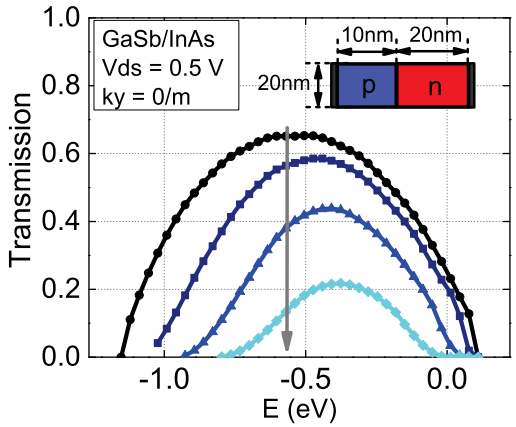

Fig. 5. Individual subband transmission probabilities at $k_y = 0$ for a broken gap diode, illustrating the transparant data analysis. Parameters have been obtained with the algorithm in Fig. 4. Doping is $5\text{x}10^{19}$ cm^{-3} in the p- and n-regions. The arrow indicates increasing subband number.

biaspoint only takes about 15 min using 10 cores on a state-of-the-art server. Fig. 6 shows the wider body device has a deteriorated SS as a result of poorer electrostatic gate control. For the 20 nm configuration, an I_{60}, the current at which the SS goes from sub-to super-60 mV/dec, of around 10 μA/μm is obtained, while I_{on} is about 150 μA/μm. The EF formalism allows for a transparent analysis of the transmission spectra of individual subband modes. Fig. 5 shows that although the band alignment is broken, the transmission is not 1, indicating reflections at the heterojunction.

V. CONCLUSION

In conclusion, we showed a full-zone 15-band EF formalism using a spectral method, along with a constrained optimization to obtain **k·p**-parameters that retain commutativity of the momentum matrices. We demonstrated the formalism for broken gap hetero-diodes and hetero-TFETs, highlighting the transparency of the analysis and the computational efficiency compared to existing QM BTBT solvers.

ACKNOWLEDGMENT

D.Verreck acknowledges support from the Agency for Innovation by Science and Technology in Flanders (IWT). This work was supported by imec's Industrial Affiliation Program.

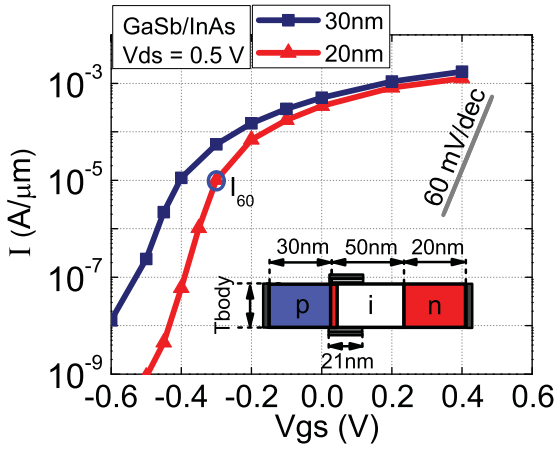

Fig. 6. QM I-V curves for broken gap p-n-i-n TFETs with Tbody 30 nm and 20 nm. One I-V curve is generated in about 2.5 h on a 10 core server, allowing for an efficient architecture optimization. Source, pocket and drain doping are $1x10^{19}$ cm^{-3}, $1x10^{19}$ cm^{-3} and $5x10^{17}$ cm^{-3} respectively. Pocket thickness is 1 nm. The gate stack has an equivalent oxide thickness of 0.6 nm and a metal workfunction of 4.5 eV.

REFERENCES

[1] H. Lu and A. Seabaugh, "Tunnel field-effect transistors: State-of-the-art," *IEEE J. Electron Dev. Soc.*, vol. 2, no. 4, pp. 44–49, July 2014.

[2] A. M. Ionescu and H. Riel, "Tunnel field-effect transistors as energy-efficient electronic switches." *Nature*, vol. 479, no. 7373, pp. 329–37, Nov. 2011.

[3] U. Avci, D. Morris, and I. Young, "Tunnel field-effect transistors: Prospects and challenges," *Electron Devices Society, IEEE Journal of the*, vol. 3, no. 3, pp. 88–95, May 2015.

[4] S. Koswatta, "On the possibility of obtaining MOSFET-like performance and sub-60-mV/dec swing in 1-D broken-gap tunnel transistors," *IEEE Trans. Electron Dev.*, vol. 57, no. 12, pp. 3222–3230, 2010.

[5] G. Dewey, B. Chu-Kung, J. Boardman, J. M. Fastenau, J. Kavalieros, R. Kotlyar, W. K. Liu, D. Lubyshev, M. Metz, N. Mukherjee, P. Oakey, R. Pillarisetty, M. Radosavljevic, H. W. Then, and R. Chau, "Fabrication, characterization, and physics of IIIV heterojunction tunneling Field Effect Transistors (H-TFET) for steep sub-threshold swing," *Int. Electron Dev. Meet.*, vol. 3, pp. 33.6.1–33.6.4, Dec. 2011.

[6] K. Tomioka and T. Fukui, "Current increment of tunnel field-effect transistor using ingaas nanowire/si heterojunction by scaling of channel length," *Appl. Phys. Lett.*, vol. 104, no. 7, pp. –, 2014.

[7] K. E. Moselund, H. Schmid, C. Bessire, M. Bjork, H. Ghoneim, and H. Riel, "Inas-si nanowire heterojunction tunnel fets," *IEEE Electron Dev. Lett.*, vol. 33, no. 10, pp. 1453–1455, Oct 2012.

[8] J. Knoch and J. Appenzeller, "Modeling of high-performance p-type IIIV heterojunction tunnel FETs," *IEEE Electron Dev. Lett.*, vol. 31, no. 4, pp. 305–307, 2010.

[9] A. W. Dey, J. Svensson, M. Ek, E. Lind, C. Thelander, and L.-E. Wernersson, "Combining axial and radial nanowire heterostructures: Radial esaki diodes and tunnel field-effect transistors," *Nano Lett.*, vol. 13, no. 12, pp. 5919–5924, 2013.

[10] M. Van de Put, "Band-to-band tunneling in III-V semiconductor heterostructures," in *EUROCON, 2013 IEEE*, 2013, pp. 2133 – 2139.

[11] D. Verreck, M. Van De Put, B. Soree, A. S. Verhulst, W. Magnus, W. G. Vandenberghe, N. Collaert, A. Thean, and G. Groeseneken, "Quantum mechanical solver for confined heterostructure tunnel field-effect transistors," *J. Appl. Phys.*, vol. 115, no. 5, pp. 053 706–053 706–8, Feb 2014.

[12] M. L. Van de Put, W. G. Vandenberghe, W. Magnus, and B. Soree, "An envelope function formalism for lattice-matched heterostructures," *Physica B: Condensed Matter*, vol. 470471, pp. 69 – 75, 2015.

[13] Y. A. Goldberg, N. M. Shmidt, and Y. A. Vul, *Handbook Series of Semiconductor Parameters*, 1999, vol. 2, ch. 3,5.

[14] S. B. Radhia, N. Fraj, I. Saidi, and K. Boujdaria, "The eight-level k . p model for the conduction and valence bands of InAs, InP, InSb," *Semicond. Sci. Technol.*, vol. 22, no. 4, p. 427, 2007.